Thermal boundary condition for the thermal lattice Boltzmann equation

G. H. Tang,* W. Q. Tao, and Y. L. He
State Key Laboratory of Multiphase Flow, School of Energy and Power Engineering, Xi'an Jiaotong University, Xi'an, Shaanxi 710049, China
(Received 6 January 2005; published 6 July 2005)

A thermal boundary condition for a double-population thermal lattice Boltzmann equation (TLBE) is introduced and numerically demonstrated. The unknown distribution population at the boundary node is decomposed into its equilibrium part and nonequilibrium parts, and then the nonequilibrium part is approximated with a first-order extrapolation of the nonequilibrium part of the populations at the neighboring fluid nodes. Numerical tests with Dirichlet and Neumann boundary constraints show that the numerical results of the TLBE together with the present boundary schemes agree well with the analytical solutions and those of the finite-volume method.

DOI: 10.1103/PhysRevE.72.016703 PACS number(s): 47.11.+j, 05.50.+q

I. INTRODUCTION

In the last 15 years or so, there has been rapid progress in developing the method of the lattice Boltzmann equation (LBE) for solving a variety of fluid dynamics problems [1–3]. This approach was first introduced by McNamara and Zanetti [4], and Higuera and Jimenez [5], Higuera and Succi [6], Qian *et al.* [7], and Chen *et al.* [8] made notable contribution in subsequent papers. There has also been an ongoing effort in the construction of stable thermal lattice Boltzmann equation (TLBE) models in order to simulate heat transfer. McNamara and Alder [9] first succeeded in simulating heat transfer phenomena by adopting multispeed thermal fluid lattice Boltzmann models. In general, the present thermal lattice Boltzmann models can be classified into three categories: the multispeed approach, the passive-scalar approach, and the double-population approach. In the multispeed approach [9–11], the internal energy term is incorporated with a density distribution function so that only the density distribution function is needed. These multispeed models suffer severe numerical instability, and the temperature variation is limited to a narrow range. In the passive-scalar thermal LBE model [12,13], the temperature is simulated using a separate distribution function which is independent of the density distribution. The main advantage of this approach is the enhancement of numerical stability. However, the viscous heat dissipation and compression work done by the pressure cannot be taken into account. In the third approach [14], an independent internal energy density distribution function was introduced to obtain the temperature field. This model has better numerical stability and the viscous heat dissipation and compression work done by the pressure can be solved fundamentally. It should be noted that the TD2G9 thermal LBE model proposed by Guo *et al.* [15] can also be classified as belonging to the third group. In addition, in the last two years, to improve the numerical stability of the TLBE further, a hybrid TLBE method has been proposed in which the mass and momentum conservation laws are solved by the usual athermal LBE, while the advection-diffusive equation satisfied by the temperature is solved separately by a finite-difference technique [16,17]. Al-Zoubi and Brenner [18] proposed a similar hybrid approach by computing the velocity and pressure field from the finite-volume method (FVM) while obtaining the temperature distribution from the LBE.

Wall boundary conditions in the LBE method were originally taken from the lattice gas automata [19–21], in which the so-called bounce-back scheme was used at walls to obtain nonslip velocity conditions. The easy implementation of this nonslip velocity condition by the bounce-back scheme supports the idea that the LBE is ideal for simulating fluid flows in complex geometries, such as flow through porous media. However, it has been confirmed that the bounce-back scheme is only of first order in numerical accuracy at the boundaries [22–24], which degrades the LBE, because the numerical accuracy of the LBE is of second order in the interior points. Other boundary treatments have been proposed to improve the numerical accuracy of the LBE. Thereinto, Ziegler [23] shifted the wall into fluid by one half mesh unit; a counterslip velocity on the wall was assumed by Inamuro *et al.* [25]; Chen *et al.* [26] proposed a second-order extrapolation scheme; Zou and He [27] extended the bounce-back condition for the nonequilibrium portion of the distribution; Guo *et al.* proposed a first-order extrapolation scheme [28]; other boundary schemes can be found in Refs. [22,24,29,30].

With regard to the thermal boundary conditions, the bounce-back rule of the nonequilibrium distribution by Zou and He [27] was applied to the thermal boundary distribution in Ref. [14]. The local thermal equilibrium distribution functions were applied on wall nodes for known wall temperatures, while the energy density distribution on the wall was set equal to those of the nearest interior nodes for adiabatic boundaries in Ref. [31]. Similar to the counterslip velocity proposed by Inamuro *et al.* [25], D' Orazio *et al.* [32,33], and D' Orazio and Succi [34] assumed a counterslip thermal energy density which is determined consistently with Dirichlet or Neumann boundary constraints. To date, there is no doubt

*Corresponding author. Electronic address: ghtang@mail.xjtu.edu.cn

that the model of assuming a counter slip thermal energy density in Refs. [32–34] is of the highest accuracy because it can guarantee the fixed velocity and temperature or heat flux at the wall exactly. However, the countertemperature assumption may cast doubt on its convenient applicability to arbitrary boundary conditions or complicated geometries [1,26,27]. Based on the idea of Guo *et al.* [15,28], in this paper we introduce a thermal boundary condition for the doubled-population TLBE model in Ref. [14] and then the two-dimensional Poiseiuille thermal flow is tested.

The outline of this paper is as follows: In Sec. II we give a brief description of the TLBE. In Sec. III we derive the thermal boundary conditions. In Sec. IV, we demonstrate some numerical simulations to validate the result, and in Sec. V we conclude the paper.

II. THERMAL LBE METHOD

The following two discrete evolution equations are needed in the TLBE model derived by He *et al.* [14] with the BGK collision model:

$$\bar{f}_i(\mathbf{r}+\mathbf{c}_i\Delta t,t+\Delta t)-\bar{f}_i(\mathbf{r},t)=-\frac{\Delta t}{\tau_f+0.5\Delta t}[\bar{f}_i(\mathbf{r},t)-f_i^{eq}(\mathbf{r},t)], \tag{1}$$

$$\bar{g}_i(\mathbf{r}+\mathbf{c}_i\Delta t,t+\Delta t)-\bar{g}_i(\mathbf{r},t)=-\frac{\Delta t}{\tau_g+0.5\Delta t}[\bar{g}_i(\mathbf{r},t)-g_i^{eq}(\mathbf{r},t)]-\frac{\tau_g\Delta t}{\tau_g+0.5\Delta t}f_iZ_i. \tag{2}$$

The new variables $\bar{f}$ and $\bar{g}$ are defined as

$$\bar{f}_i=f_i+\frac{0.5\Delta t}{\tau_f}(f_i-f_i^{eq}), \tag{3}$$

$$\bar{g}_i=g_i+\frac{0.5\Delta t}{\tau_g}(g_i-g_i^{eq})+\frac{\Delta t}{2}f_iZ_i, \tag{4}$$

where f and g are the density distribution function and the internal energy density distribution function, respectively; f^{eq} and g^{eq} are their corresponding equilibrium functions; τ_f and τ_g are the momentum and internal energy relaxation time, respectively; $\mathbf{c}_i$ is the lattice velocity, and i denotes the lattice direction; Δx and Δt are the lattice spacing and time step,

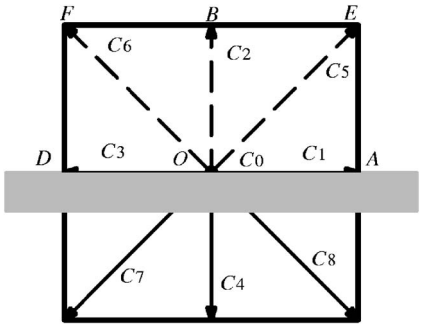

FIG. 1. Schematic plot of velocity directions at a wall boundary.

respectively; $\mathbf{r}$ denotes the coordinate vector. The term $Z_i=(\mathbf{c}_i-\mathbf{u})\cdot[\partial\mathbf{u}/\partial t+(\mathbf{c}_i\cdot\nabla)\mathbf{u}]$ represents the effect of viscous heating and can be expressed as [34]

$$Z_i=\frac{(\mathbf{c}_i-\mathbf{u})\cdot[\mathbf{u}(\mathbf{r}+\mathbf{c}_i\Delta t,t+\Delta t)-\mathbf{u}(\mathbf{r},t)]}{\Delta t}. \tag{5}$$

For the D2Q9 lattice [two-dimensional (2-D) and nine-velocity] with $c=\sqrt{3RT_0}$, where T_0 is the average temperature, the equilibrium density distributions are chosen as follows:

$$f_i^{eq}=\rho\omega_i\left[1+\frac{3(\mathbf{c}_i\cdot\mathbf{u})}{c^2}+\frac{9(\mathbf{c}_i\cdot\mathbf{u})^2}{2c^4}-\frac{3(\mathbf{u}\cdot\mathbf{u})}{2c^2}\right], \tag{6}$$

$$g_0^{eq}=\omega_0\rho e\left(-\frac{3\mathbf{u}\cdot\mathbf{u}}{2c^2}\right),$$

$$g_i^{eq}=\omega_i\rho e\left[\frac{3}{2}+\frac{3(\mathbf{c}_i\cdot\mathbf{u})}{2c^2}+\frac{9(\mathbf{c}_i\cdot\mathbf{u})^2}{2c^4}-\frac{3(\mathbf{u}\cdot\mathbf{u})}{2c^2}\right],$$

$$i=1,2,3,4,$$

$$g_i^{eq}=\omega_i\rho e\left[3+\frac{6(\mathbf{c}_i\cdot\mathbf{u})}{c^2}+\frac{9(\mathbf{c}_i\cdot\mathbf{u})^2}{2c^4}-\frac{3(\mathbf{u}\cdot\mathbf{u})}{2c^2}\right],$$

$$i=5,6,7,8, \tag{7}$$

where ω_i is the weighting coefficient and $\omega_0=4/9$, $\omega_i=1/9$ for $i=1$, 2, 3, 4 and $\omega_i=1/36$ for $i=5$, 6, 7, 8. The internal energy density is $\rho e=\rho RT$ (in 2D). The lattice velocity for the D2Q9 lattice is

$$\mathbf{c}_i=\begin{cases}0, & i=0,\\ \left(\cos\left[\frac{(i-1)\pi}{2}\right],\sin\left[\frac{(i-1)\pi}{2}\right]\right)c, & i=1,2,3,4,\\ \sqrt{2}\left(\cos\left[(i-5)\frac{\pi}{2}+\frac{\pi}{4}\right],\sin\left[(i-5)\frac{\pi}{2}+\frac{\pi}{4}\right]\right)c, & i=5,6,7,8.\end{cases} \tag{8}$$

Finally, the macroscopic density ρ, velocity $\mathbf{u}$, internal energy per unit mass e, heat flux $\mathbf{q}$, kinematic viscosity ν, and thermal diffusivity a can then be obtained from the following equations [14,34]:

$$\rho = \sum_i \bar{f}_i, \quad \rho\mathbf{u} = \sum_i \bar{f}_i \mathbf{c}_i, \quad \rho e = \sum_i \bar{g}_i - \frac{\Delta t}{2}\sum_i f_i Z_i,$$

$$\mathbf{q} = \left(\sum_i \mathbf{c}_i \bar{g}_i - \rho e\mathbf{u} - \frac{\Delta t}{2}\sum_i \mathbf{c}_i f_i Z_i\right)\frac{\tau_g}{\tau_g + 0.5\Delta t},$$

$$\nu = \tau_f RT_0, \quad a = 2\tau_g RT_0. \tag{9}$$

III. VELOCITY AND THERMAL BOUNDARY CONDITIONS

As proposed in Ref. [28], for the velocity boundary condition at the wall, in which the momentum distribution function at the boundary node is decomposed into its equilibrium and nonequilibrium parts and in Ref. [15] for the thermal boundary conditions, the internal energy distribution function at the boundary node decomposed into its equilibrium and nonequilibrium parts is adopted here. The nonequilibrium part is approximated with a first-order extrapolation of the nonequilibrium part of the distribution at the nearest interior fluid node. For illustration and simplicity, we consider the case of a flat boundary and report the procedure described in Ref. [28], as applied to the thermal population of the present scheme. As shown in Fig. 1, the *DOA* line lies at the boundary, and the nodes F, B, and E are those lying in the fluid. Note that one evolution equation of the LBE, consists of two computational steps

$$\text{collision: } \bar{g}_i^*(\mathbf{r},t) = (1-\omega_g)\bar{g}_i(\mathbf{r},t) + \omega_g g_i^{eq}(\mathbf{r},t) - \omega_g \tau_g f_i Z_i,$$

$$\text{streaming: } \bar{g}_i(\mathbf{r}+\mathbf{c}_i\Delta t, t+\Delta t) = \bar{g}_i^*(\mathbf{r},t), \tag{10}$$

where we use ω_g to replace $\Delta t/(\tau_g+0.5\Delta t)$ for simplicity. Obviously, $\bar{g}_i^*(O,t)$ needs to finish the streaming step for $i=2$, 5, and 6 at the boundary node O. Notice that the distribution function $\bar{g}_i(\mathbf{r},t)$ can be decomposed into its equilibrium and nonequilibrium parts

$$\bar{g}_i(\mathbf{r},t) = g_i^{eq}(\mathbf{r},t) + g_i^{neq}(\mathbf{r},t), \tag{11}$$

where $g_i^{neq}(\mathbf{r},t)$ is the nonequilibrium part of $\bar{g}_i$. Thus the post-collision distribution at the boundary node, $\bar{g}_i^*(O,t)$, can be rewritten as

$$\bar{g}_i^*(O,t) = g_i^{eq}(O,t) + (1-\omega_g)g_i^{neq}(O,t) - \omega_g\tau_g f_i Z_i. \tag{12}$$

First we discuss how to calculate the nonequilibrium part. By using the Chapman-Enskog method or the multiscaling expansion for the lattice Boltzmann equation, we assume that $g_i^{neq} = \varepsilon g_i^{(1)}$, where ε is the expansion parameter. At time t, the macroscopic velocity and pressure and density of the flow are known at the fluid node B, so $g_i^{eq}(B,t)$ can be determined, and thus the nonequilibrium part of the distribution at node B can be given by

$$g_i^{neq}(B,t) = g_i(B,t) - g_i^{eq}(B,t). \tag{13}$$

Also note that $g_i^{(1)}(O,t) = g_i^{(1)}(B,t) + O(\varepsilon)$, and $g_i^{neq}(O,t)$ can be approximated by a first-order extrapolation

$$g_i^{neq}(O,t) = g_i(B,t) - g_i^{eq}(B,t) + O(\varepsilon^2). \tag{14}$$

Equation (14) implies that the accuracy of the approximation of $g_i^{neq}(O,t)$ with the first-order extrapolation scheme based on $g_i^{neq}(B,t)$ is indeed of second-order.

Now we discuss the determination of the equilibrium part $g_i^{eq}(O,t)$. For the velocity and temperature condition in which $\mathbf{u}(O,t)$ and $T(O,t)$ are known and $\rho(O,t)$ is unknown, we approximate $g_i^{eq}(O,t)$ as the following form by substituting the density of the nearest internal node for that of the boundary node:

$$g_i^{eq}(O,t) = g_i^{eq}(\rho(B), \mathbf{u}(O), T(O), t). \tag{15}$$

Therefore, we can obtain the final expression of the collision step:

$$\bar{g}_i^*(O,t) = g_i^{eq}(\rho(B), \mathbf{u}(O), T(O), t) + (1-\omega_g)[g_i(B,t) - g_i^{eq}(B,t)] - \omega_g\tau_g f_i(O)Z_i(O). \tag{16}$$

If the wall is a Neumann boundary—i.e., the wall heat flux is known—we can use the expression of $\mathbf{q}$ (see Eq. (9)), together with Eqs. (6) and (16) to obtain the wall temperature expression $T(O,t)$ first. For example, for a fixed bottom wall where the flow velocity is zero and $\bar{g}_4, \bar{g}_7$, and $\bar{g}_8$ are known at boundary node O (for the D2Q9 lattice), the wall temperature is calculated from the equation

$$T(O) = \frac{1}{R\rho(B)(1.5\omega_2 + 3\omega_5 + 3\omega_6)}\left[q_y\frac{\tau_g + 0.5\Delta t}{\tau_g} + \frac{\Delta t}{2}\sum_i \mathbf{c}_i f_i(O)Z_i(O) + \sum_{i=4,7,8}\mathbf{c}_i\bar{g}_i - [(1-\omega_g)(g_i(B,t) - g_i^{eq}(B,t)) - \omega_g\tau_g f_i(O)Z_i(O)]\right]. \tag{17}$$

Then we use Eq. (16) to calculate the unknown populations of $\bar{g}_2, \bar{g}_5$, and $\bar{g}_6$.

Similar to the scheme for thermal boundary conditions, the velocity boundary condition has the expression

$$\bar{f}_i^*(O,t) = f_i^{eq}(\rho(B), \mathbf{u}(O), t) + (1-\omega_f)[f_i(B,t) - f_i^{eq}(B,t)], \tag{18}$$

where $\omega_f = \Delta t/(\tau_f + 0.5\Delta t)$.

IV. NUMERICAL RESULTS

A two-dimensional plane flow with the walls at rest is considered. Uniform velocity and temperature profiles U_{in} and T_{in}, at the inlet section, and hydrodynamic and thermally fully developed flow, at the outlet section, are imposed. Three types of thermal boundary conditions usually encountered in the engineering applications at the plane walls are applied. In the first boundary condition, the lower and upper

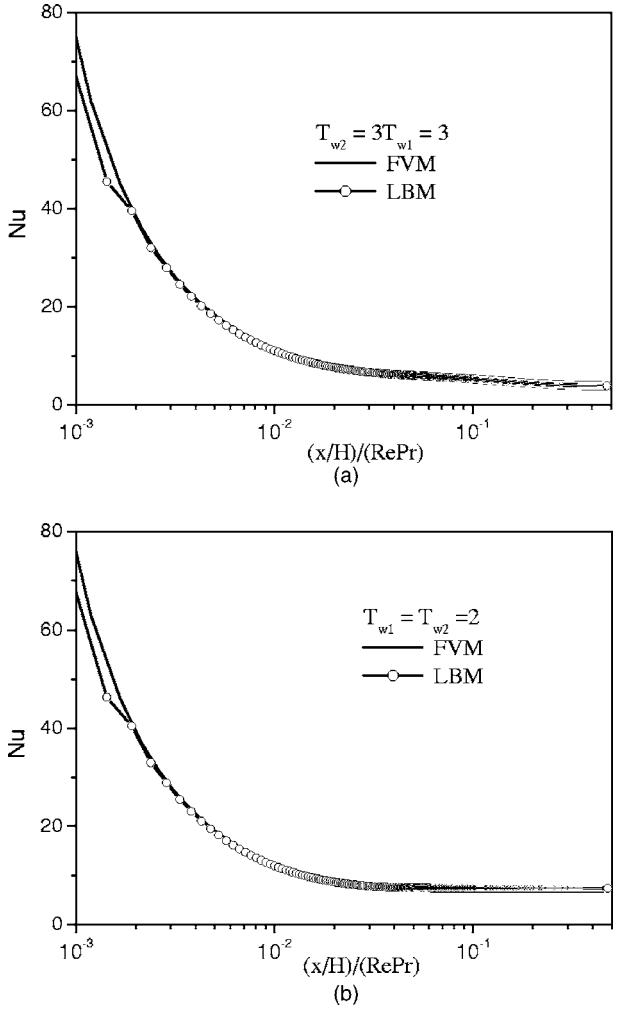

FIG. 2. Local Nusselt number distribution along the streamwise direction for the first type thermal boundary condition. The solid lines represent the numerical results of the finite-volume method, and the circles plus lines represent the results of the present thermal lattice Boltzmann equation. (a) $T_{in}=5, T_{w1}=1, T_{w2}=3, \tau_f=0.2, \tau_g=0.143$. (b) $T_{in}=5, T_{w1}=T_{w2}=2, \tau_f=0.2, \tau_g=0.143$.

walls keep at uniform temperature T_{w1} and T_{w2}, respectively. In the second boundary condition, the lower and upper walls keep at uniform heat flux q_{w1} and q_{w2}, respectively. In the third boundary condition, the lower wall keeps at uniform temperature T_{w1} and the upper wall keeps at uniform heat flux q_{w2}, respectively.

A 1001×101 grid, corresponding to an aspect ratio $L/H=10$, is used. The average temperature T_0 is $T_0=(T_{in}+T_{w1}+T_{w2})/3$ for the first type thermal boundary condition, $T_0=T_{in}$ for the second type, and $T_0=(T_{in}+T_{w1})/2$ for the third type. During simulations, the Prandtl number is fixed at $\mathrm{Pr}=0.7$ and inlet velocity is fixed at $U_{in}=0.01$ for all the cases. The present nonequilibrium extrapolation scheme is applied at the entrance and upper and lower walls for velocity and thermal boundaries. The unknown distribution functions at the outlet are extrapolated from the interior flow field (the first layer and second layer inside the fluid) [26].

The Nusselt number as a function of the Graetz number, $\mathrm{RePr}/(x/H)$, is shown in Figs. 2–4. The local Nusselt num-

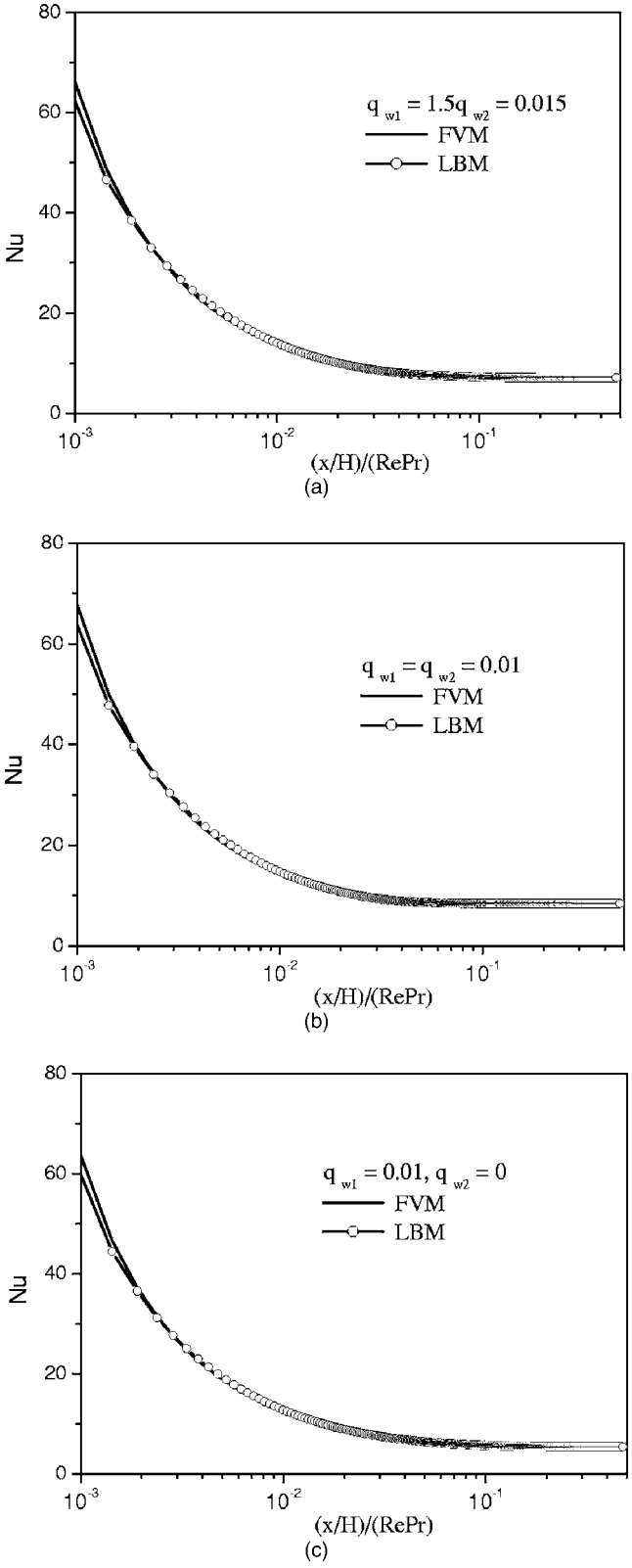

FIG. 3. Local Nusselt number distribution along the streamwise direction for the second type thermal boundary condition. The solid lines represent the numerical results of the finite-volume method, and the circles plus lines represent the results of the present thermal lattice Boltzmann equation. (a) $T_{in}=1, q_{w1}=0.015, q_{w2}=0.01, \tau_f=0.2, \tau_g=0.14$. (b) $T_{in}=1, q_{w1}=q_{w2}=0.01, \tau_f=0.2, \tau_g=0.14$. (c) $T_{in}=1, q_{w1}=0.01, q_{w2}=0, \tau_f=0.2, \tau_g=0.14$.

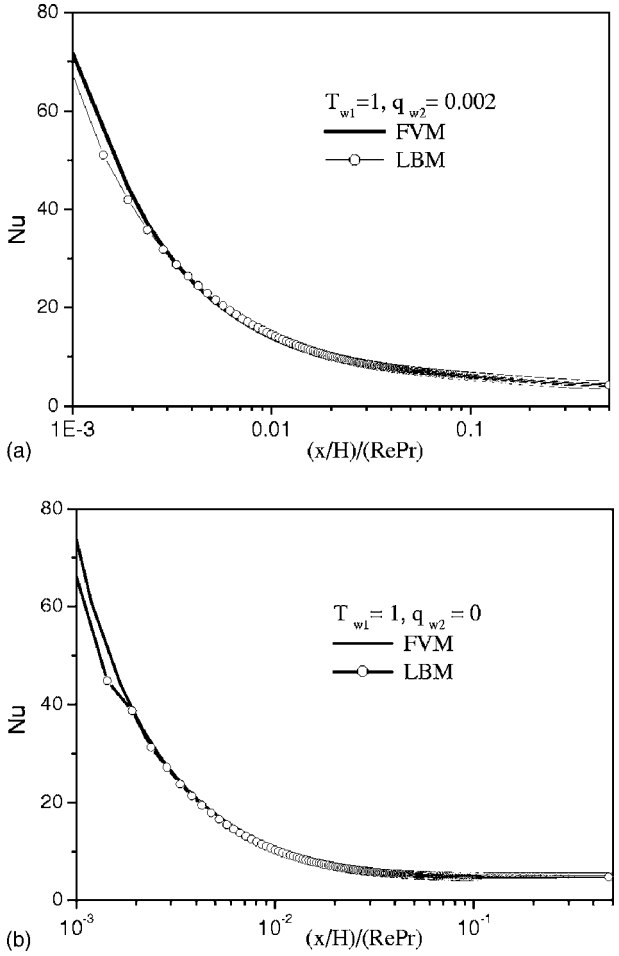

FIG. 4. Local Nusselt number distribution along the streamwise direction for the third thermal boundary condition. The solid lines represent the numerical results of the finite-volume method, and the circles plus lines represent the results of the present thermal lattice Boltzmann equation. (a) $T_{in}=5, T_{w1}=1, q_{w2}=0.002, \tau_f=0.2, \tau_g=0.143$. (b) $T_{in}=5, T_{w1}=1, q_{w2}=0, \tau_f=0.2, \tau_g=0.143$.

ber is defined as $\mathrm{Nu}_x=D_h q_{w,x}/[\lambda(T_{w,x}-T_{b,x})]$, where D_h is the hydraulic diameter of the channel, $q_{w,x}=\lambda(\partial T_x/\partial y)_w$ is the wall local heat flux, λ is the thermal conductivity, and $T_{b,x}=\int_0^H \rho u T dy/\int_0^H \rho u dy$ is the bulk temperature. The numerical results of the finite-volume method are also shown in the figures for comparison. Except for several nodes near the inlet, the results of both methods coincide perfectly for all the tested cases, which verify the implementation of the boundary conditions. In the present simulation, like most boundary treatments, the scheme for solid wall is directly extended to the inlet boundary with known velocity and temperature. However, according to Yu *et al.* [2], the interaction between the inlet boundary and the interior of the flow field may have an effect on the quality of the solution. An improved treatment on the inlet boundary condition is required to minimize the impact (see Ref. [2] for further details). From the figures we can also observe that the predicted thermal entry length of the LBE is in good agreement with the result of the FVM. In the limit of large inverse Graetz numbers—i.e., for a thermally fully developed flow—the predicted Nusselt numbers at the lower plane compared with

TABLE I. Comparison of the Nusselt numbers at the lower plane in the thermal fully developed region.

Thermal boundary condition		Analytical	LBM
First type	$T_{w1}\neq T_{w2}$	4	3.93
	$T_{w1}=T_{w2}$	7.54	7.67
Second type	$q_{w1}=1.5q_{w2}$	7.0	7.09
	$q_{w1}=q_{w2}$	8.24	8.39
	$q_{w2}=0$	5.38	5.42
Third type	$q_{w2}\neq 0$	4	4.07
	$q_{w2}=0$	4.86	4.79

the analytical solutions [35] are shown in Table I. The deviation is less than 2% for all cases considered. It is noted that for the second type thermal boundary, the analytical solutions for the Nusselt number are calculated using $\mathrm{Nu}_1=140/[26-9(q_{w2}/q_{w1})]$ at the lower wall with uniform heat flux q_{w1} and $\mathrm{Nu}_2=140/[26-9(q_{w1}/q_{w2})]$ at the upper wall with uniform heat flux q_{w2}. The analytical solutions are 4.0 for both the first type condition T_{w1} not equal T_{w2} and the third type condition q_{w2} not zero. Figure 5 shows the normalized temperature profiles at the channel outlet section. The squares, circles, and triangles represent the present TLBE results for $T_{w2}=3T_{w1}, T_{w2}=T_{w1}$, and $q_{w2}=0$, respectively. The solid lines represent corresponding numerical results of the finite-volume method. We can see that the TLBE predictions agree well with the numerical results of the finite-volume method.

V. CONCLUSIONS

In this paper we have proposed a method to implement thermal boundary conditions [15,28] for the TLBE [14]. The basic idea is to decompose the distribution function at the

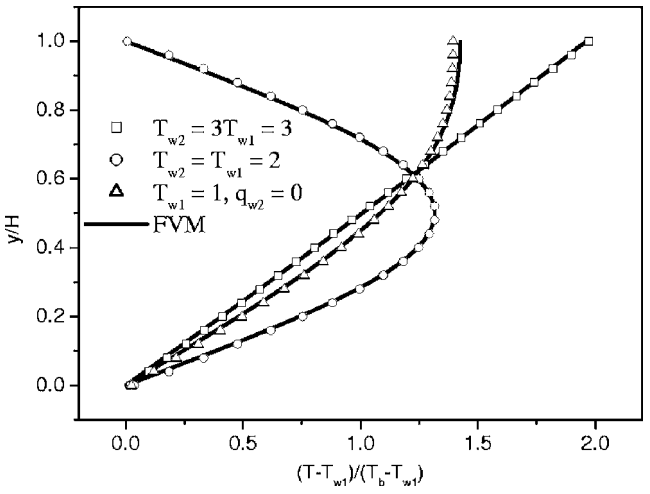

FIG. 5. Normalized temperature profiles at the channel outlet section for different thermal boundary conditions. The squares, circles, and triangles represent the TLBE results for $T_{w2}=3T_{w1}, T_{w2}=T_{w1}$, and $q_{w2}=0$, respectively. The solid lines represent corresponding numerical results of the finite-volume method.

boundary node into its equilibrium and nonequilibrium parts. The nonequilibrium part is approximated by extrapolating from the nonequilibrium distribution at the neighboring fluid node and the first-order extrapolation is proved to be of second-order accuracy for flat boundaries [26,28]. The numerical test results with the double-population TLBE approach for two-dimensional Poiseuille flow show that the TLBE solutions using the present boundary conditions are in good agreement with the analytical solutions and those of the finite-volume method. In the present boundary condition, we only perform the first-order extrapolation for both velocity population and thermal population. It has been verified to be of better numerical stability than the second-order extrapolation scheme for velocity boundary condition in Ref. [28]. The present extropolation scheme could be convenient to implement for complicated geometries. The study of heat transfer in porous media with the present thermal boundary condition will be reported in future work. In addition, by applying a hybrid TLBE method [16–18] in which the momentum equation or temperature equation is solved by finite-difference methods, the present velocity or thermal boundary conditions can be adapted to situations of engineering interest.

ACKNOWLEDGMENTS

This research was supported by the National Natural Science Foundation of China (Grant No. 50406020), the National Science Fund for Distinguished Young Scholars from the National Natural Science Foundation of China (Grant No. 50425620).

[1] S. Y. Chen and G. D. Doolen, Annu. Rev. Fluid Mech. **30**, 329 (1998).
[2] D. Z. Yu, R. W. Mei, L. S. Luo, and W. Shyy, Prog. Aerosp. Sci. **39**, 329 (2003).
[3] S. Succi, *Lattice Boltzmann Equation for Fluid Dynamics and Beyond* (Clarendon Press, Oxford, 2001).
[4] G. McNamara and G. Zanetti, Phys. Rev. Lett. **61**, 2332 (1988).
[5] F. J. Higuera and J. Jimenez, Europhys. Lett. **9**, 663 (1989).
[6] F. J. Higuera and S. Succi, Europhys. Lett. **8**, 517 (1989).
[7] Y. H. Qian, D. d'Humieres, and P. Lallemand, Europhys. Lett. **17**, 479 (1992).
[8] S. Chen, H. D. Chen. D. Martinez, and W. H. Matthaeus, Phys. Rev. Lett. **67**, 3776 (1991).
[9] G. McNamara and B. Alder, Physica A **194**, 218 (1993).
[10] F. J. Alexander, S. Chen, and J. D. Sterling, Phys. Rev. E **47**, R2249 (1993).
[11] Y. Chen, H. Ohashi, and M. Akiyama, Phys. Rev. E **50**, 2776 (1994).
[12] X. Shan, Phys. Rev. E **55**, 2780 (1997).
[13] J. G. M. Eggels and J. A. Somers, Int. J. Heat Fluid Flow **16**, 357 (1995).
[14] X. Y. He, S. Y. Chen, and G. D. Doolen, J. Comput. Phys. **146**, 282 (1998).
[15] Z. L. Guo, B. C. Shi, and C. G. Zheng, Int. J. Numer. Methods Fluids **39**, 325 (2002).
[16] P. Lallemand and L. S. Luo, Phys. Rev. E **68**, 036706 (2003).
[17] P. Lallemand and L. S. Luo, Int. J. Mod. Phys. B **17**, 41 (2003).
[18] A. Al-Zoubi and G. Brenner, Int. J. Mod. Phys. C **15**, 307 (2004).
[19] J. Hardy, O. D. Pazzis, and Y. Pomeau, Phys. Rev. A **13**, 1949 (1976).
[20] U. Frisch, B. Hasslacher, and Y. Pomeau, Phys. Rev. Lett. **56**, 1505 (1986).
[21] U. Frisch, D. d'Humieres, B. Hasslacher, P. Lallemand, Y. Pomeau, and J. P. Rivet, Complex Syst. **1**, 649 (1987).
[22] R. Cornubert, D. d'Humieres, and D. Levermore, Physica D **47**, 241 (1991).
[23] D. P. Ziegler, J. Stat. Phys. **71**, 1171 (1993).
[24] X. Y. He, Q. S. Zou, L. S. Luo, and M. Dembo, J. Stat. Phys. **87**, 115 (1997).
[25] T. Inamuro, M. Yoshino, and F. Ogino, Phys. Fluids **7**, 2928 (1995).
[26] S. Y. Chen, D. Martinez, and R. W. Mei, Phys. Fluids **8**, 2527 (1996).
[27] Q. S. Zou and X. Y. He, Phys. Fluids **9**, 1591 (1997).
[28] Z. L. Guo, C. G. Zheng, and B. C. Shi, Chin. Phys. **11**, 366 (2002).
[29] P. A. Skordos, Phys. Rev. E **48**, 4823 (1993).
[30] D. R. Noble, S. Y. Chen, J. G. Georgiadis, and R. O. Buckius, Phys. Fluids **7**, 203 (1995).
[31] G. H. Tang, W. Q. Tao, and Y. L. He, Int. J. Mod. Phys. B **17**, 183 (2003).
[32] A. D' Orazio, S. Succi, and C. Arrighetti, Phys. Fluids **15**, 2778 (2003).
[33] A. D' Orazio, M. Corcione, and G. P. Celata, Int. J. Therm. Sci. **43**, 575 (2004).
[34] A. D' Orazio and S. Succi, Future Generation Comput. Syst. **20**, 935 (2004).
[35] R. K. Shah and A. L. London, *Advances in Heat Transfer* (Academic Press, New York, 1978), Suppl. 1.

Errata

$$T(O)=\frac{1}{R\rho(B)(1.5\omega_2+3\omega_5+3\omega_6)}\left(\begin{array}{l} q_y\dfrac{\tau_g+0.5\Delta t}{\tau_g}+\dfrac{\Delta t}{2}\sum_i \mathbf{c}_{iy} f_i(O)Z_i(O)+\sum_{i=4,7,8}\mathbf{c}_{iy}\overline{g_i}- \\ \sum_{i=2,5,6}\left[(1-\omega_g)\left(g_i(B,t)-g_i^{eq}(B,t)\right)-\omega_g\tau_g f_i(O)Z_i(O)\right] \end{array}\right) \quad (17)$$